Lab on a Chip

Integrated Microfluidic Multiple Electrode Aggregometry for Point-of-Care Platelet Function Analysis

Journal:	*Lab on a Chip*
Manuscript ID	LC-ART-05-2024-000469.R1
Article Type:	Paper
Date Submitted by the Author:	20-Aug-2024

Complete List of Authors:	Zhao, Xin; Shanghai Jiao Tong University, Department of Electronic Engineering Gopal, Vineeth; Atantares Corp Lozano-Juan, Ferran; Atantares Corp, Kolandaivelu, Kumaran; Atantares Corp; Massachusetts Institute of Technology, Institute for Medical Engineering and Science; Brigham and Women's Hospital, Cardiovascular Division Sarkar, Aniruddh; Georgia Institute of Technology, Biomedical Engineering; Emory University, Biomedical Engineering Wu, Dan; Atantares Corp, Su, Jianzhou; Atantares Corp Cheng, Qingyuan; Shanghai Jiao Tong University, Department of Electronic Engineering Pang, Ruoying; Shanghai Jiao Tong University, Department of Electronic Engineering Wu, Lin-Sheng; Shanghai Jiao Tong University, Department of Electronic Engineering

Integrated Microfluidic Multiple Electrode Aggregometry for Point-of-Care Platelet Function Analysis

X. Zhao[1,2*†], V. R. Gopal[2*], F. Lozano-Juan[2*], K. Kolandaivelu[3,4], A. Sarkar[5], D. Wu[2], J. Su[2], Q. Cheng[1], R, Pang[1], L.-S. Wu[1]

[1]State Key Laboratory of Radio Frequency Heterogeneous Integration, Shanghai Jiao Tong University, Shanghai, China

[2]Atantares Corp., One Broadway, Cambridge, MA, USA

[3]Institute for Medical Engineering and Science, Massachusetts Institute of Technology, Cambridge, MA, USA

[4]Cardiovascular Division, Brigham and Women's Hospital, Boston, MA, USA

[5]Wallace H. Coulter Department of Biomedical Engineering, Georgia Institute of Technology, Atlanta, GA, USA

*These authors contributed equally to this work.

†Corresponding Author: X. Zhao, 800 Dongchuan Road, Minhang District, Shanghai 200240, Email: xinzhao@sjtu.edu.cn

Abstract:

Point-of-care (POC) platelet function analysis can enable timely and precise management of bleeding and clotting in emergency rooms, operation rooms and intensive care units. However, POC platelet testing is currently not commonly performed, due to the complexity of sample preparation and limitations of existing technologies. Here, we report the development of an integrated microfluidic multiple electrode aggregometry (μMEA) sensor which uses multi-frequency impedance measurement of an embedded microelectrode array to perform platelet aggregometry directly from whole blood, sensing and measuring platelet activation in a label-free manner and without requiring any additional sample preparation. Additionally, the sensor incorporates blood flow during the assay to account for physiological flow and shear conditions. We show that the impedance signal from the sensor can be used to accurately detect and quantify platelet aggregation in a label-free manner, which was further validated by simultaneous fluorometric measurement and visualization of platelet aggregation. Further, we optimized the sensitivity and repeatability of the sensor using its frequency response and demonstrated that the sensor could be used to characterize drug dose-response in antiplatelet therapy with a frequency-tunable dynamic range. We also demonstrate that the sensor provides high sensitivity to perform platelet aggregometry under thrombocytopenic or low platelet count conditions. The μMEA sensor could thus enable POC platelet function analysis across several clinical applications.

1. Introduction

Thrombosis, the formation of a blood clot, relies on the synergy of multiple cellular and protein pathways[1]. This multifactorial nature makes it challenging to diagnose and manage clotting and bleeding in acute care settings such as emergency rooms, operating rooms, and intensive care units (ICU). In these settings, point-of-care (POC) testing can provide real-time information for rapid clinical decision making[2]. Platelets are one of the key players in the clotting process, responsible for forming the primary platelet plug and facilitating protein adhesion. However, POC measurement of platelet function is currently not commonly performed, in part due to the complexity of sample preparation and limitations of current instrumentation. Microscale sensors and microfluidics provide a unique opportunity to develop integrated, miniaturized, and multiplexed POC systems. To this end, we introduce a microscale POC platform to measure platelet function which is termed as the Microfluidic Multiple Electrode Aggregometry (μMEA).

The current gold standard in measuring platelet aggregation is light transmission aggregometry (LTA), which assesses platelet aggregation via light transmission in platelet-rich plasma samples[3,4]. However, LTA is not suitable for whole blood samples as the opacity of whole blood makes it difficult to discriminate the status (i.e., activated, or inactive) of platelets in the sample through light transmission. Recently, microfluidic techniques[5] have been applied for automatic sample preparation required to isolate platelet-rich plasma. Still, these additional steps add complexity and cost, and more importantly, makes LTA unable to account for extracellular interactions present in-vivo[6].

Multiple electrode aggregometry (MEA) directly measures platelet aggregation in whole blood through electrical impedance measured using two sets of paired wire electrodes immersed in a vial of blood. However, conventional MEA systems do not account for physiological blood flow and shear conditions[7–11]. Flow is a critical variable to be considered when studying thrombus formation due to the ramifications on material transport[12] to and from the thrombus as well as the various shear-dependent processes such as platelet tethering, shear activation and microaggregate formation[13-15]. This has led to the development of multiple microfluidic shear-activated platelet function testing devices[16-19]. The requirement of bulky and

expensive optical systems such as microscope in these methods makes them unsuitable for POC applications. Another challenge faced by conventional MEA is thrombocytopenia, or low platelet count, seen in up to 60% of patients admitted to the ICU[20]. Traditional metrics of aggregation (e.g. Area under the Curve or AUC in MEA) are difficult to interpret when platelet counts fall below 150,000/μL and especially below 75,000/μL due to low signal-to-noise ratio[21].

To address the above challenges, we develop the μMEA platform where an array of microfabricated electrodes for label-free impedance aggregometry is integrated within a microfluidic channel. The μMEA chip has a significantly larger electrode surface area to chamber volume ratio than conventional MEA systems enabling efficient capture of platelets. The microfluidic blood flow enables enhanced platelet transport over the electrode surface and precise control of the local shear rate experienced by the platelets. Combined, these features promise enhanced sensitivity in platelet aggregation analysis. Here, we first report the design and fabrication of the multiplexed μMEA platform. We then verify its use in measuring platelet aggregation from whole human blood and optimize the measurement sensitivity and repeatability. Finally, we demonstrate the application of the μMEA platform in two clinically relevant scenarios: the measurement of anti-platelet drug responses and the measurement of platelet aggregation in low platelet count samples modeling thrombocytopenia.

2. Materials and Methods

*μ*MEA Sensor Fabrication

The μMEA microelectrode pattern was designed in AutoCAD (Autodesk, Inc). Gold microelectrodes (100nm) on a Titanium adhesion layer (10nm) were then patterned onto the surface of a glass wafer substrate (0.5mm thick, UniversityWafer) using standard photolithography and lift-off techniques. The glass wafer was then diced into individual chips. Microfluidic channels with a thin rectangular cross-section (height, h = 50μm, width w = 2.1mm, length, l = 7.2mm) were prepared using soft lithography of PDMS[22]. A custom mold made by laser cutting Kapton tape on a silicon wafer base was used to cast the Sylgard 184 PDMS prepolymer (Dow Corning, Sigma Aldrich). The PDMS was then cured at

65℃ for 4 hours, peeled off the molds and then cut into pieces. Using standard biopsy punches, an inlet was made by punching halfway from the channel end with a 0.3mm punch and then punching from the opposite side with a 1.5mm punch. A 1.5mm outlet was then punched into each piece after which they were aligned, and plasma bonded to the glass μMEA microelectrode chips. Lastly, to complete sensor assembly, the bonded chips were then glued, and wire bonded to individual small, printed circuit boards referred to here as 'daughter boards' that were designed to be easily mounted onto a circuit motherboard which enabled multiplexed measurements.

Sensor Setup and Operation

Tygon™ tubing (0.02"/0.51mm ID × 0.06"/1.52mm OD, Saint-Gobain, Fisher Scientific) was inserted into the inlets and outlets of individual sensors. Bubble-free and leak-free priming was performed by pushing 1X PBS buffer (Sigma Aldrich) from the outlet using a syringe. After this, the syringe was loaded into one of the channels of a Chemyx Nexus 3000 Syringe Pump and the daughter boards were plugged into the motherboard. Impedance measurements were performed using an Agilent E4980 LCR meter interfaced to a computer via a custom MATLAB script, capable of real time display and saving of data. The inlet tube was then dipped into a central stirred vial of blood.

Human blood collected into Sodium Heparin (1000U/mL) vacutainers were purchased directly from Research Blood Components LLC (Watertown, MA USA). All the volunteers gave informed consent to use their blood for research. Our blood experiment was conducted under MIT Institute for Medical Engineering and Science IRB protocol. The blood was diluted with 1XPBS buffer to a (1:4) ratio and supplemented with the thrombin inhibitor D-phenylalanyl-L-prolyl-L-arginine chloromethyl ketone dihydrochloride (PPACK, 80μM final concentration, Sigma-Aldrich)[23] to further prevent the formation of blood clots. The syringe pump, magnetic stirrers and LCR meter were controlled via a computer and started simultaneously to perform the measurement. Blood was drawn into the sensor via the syringe pump at a controlled flow rate (50 - 100μL/min) until a stable baseline was reached, after which the activator ADP (Adenosine diphosphate, 5uM, Sigma Aldrich) was added to the blood vial. ADP was

chosen due to its pathophysiological role in heart attack and strokes[24]. While studying anti-platelet drug dose response, 5μL of Cangrelor (100nM, SigmaAldrich) was added into the reagent pool in addition to the activator.

The raw impedance signal was translated into metrics such as percentage difference and AUC. Percentage difference was computed by computing the magnitude of the impedance change post-activation as a percentage of the average baseline impedance value. AUC was calculated by integrating the curve using the trapezoidal method via the trapz function in MATLAB.

Fluorescence Imaging

Fluorescence imaging was used to confirm platelet aggregation on the μMEA chip surface. Platelets in whole blood were labelled using Mepacrine (1mM Quinacrine Hydrochloride, Sigma Aldrich)[25] and observed under UV illumination with a Quinacrine filter. The μMEA chip surface was then imaged with impedance measurements occurring concurrently. The correlation between the impedance and microscopy data sets was then calculated using Graphpad Prism.

Preparation of Thrombocytopenic Blood Model

A thrombocytopenic blood model was prepared according to literature[26,27]. Whole blood was centrifuged at 300g for 8 minutes after which, the platelet rich plasma was carefully removed and replaced with an equivalent volume of 1X PBS buffer. To confirm that low platelet counts had been achieved while maintaining hematocrit, the samples were sent for analysis via a complete blood count (CBC, LabCorp). The blood model was treated identically to healthy whole blood samples, following the procedure outlined earlier. A higher concentration of ADP (20μM) was used for platelet activation when testing sensor performance in thrombocytopenic conditions.

3. Results and Discussion

Device Design, Setup and Operation

The µMEA sensor was designed to detect platelet aggregation from flowing whole blood using electrical impedance measurements produced by surface adhesion of activated platelets across the electrode array. Here we discuss the details of ~~the~~ how the device was designed, fabricated, and operated. As shown in Fig. 1(A), the µMEA sensor consists of a PDMS microfluidic channel, and the µMEA chip which was created by patterning an interdigitated microelectrode array (Fig. 1(B)) on a glass substrate. The channel was bonded to the chip such that the electrodes were aligned at the center of the channel to minimize flow entrance and exit effects. The µMEA sensor (i.e. the assembly of the channel and the electrode) is then assembled onto a custom printed circuit board to enable 'plug-and-play' use during testing (Fig. 1(A)). Up

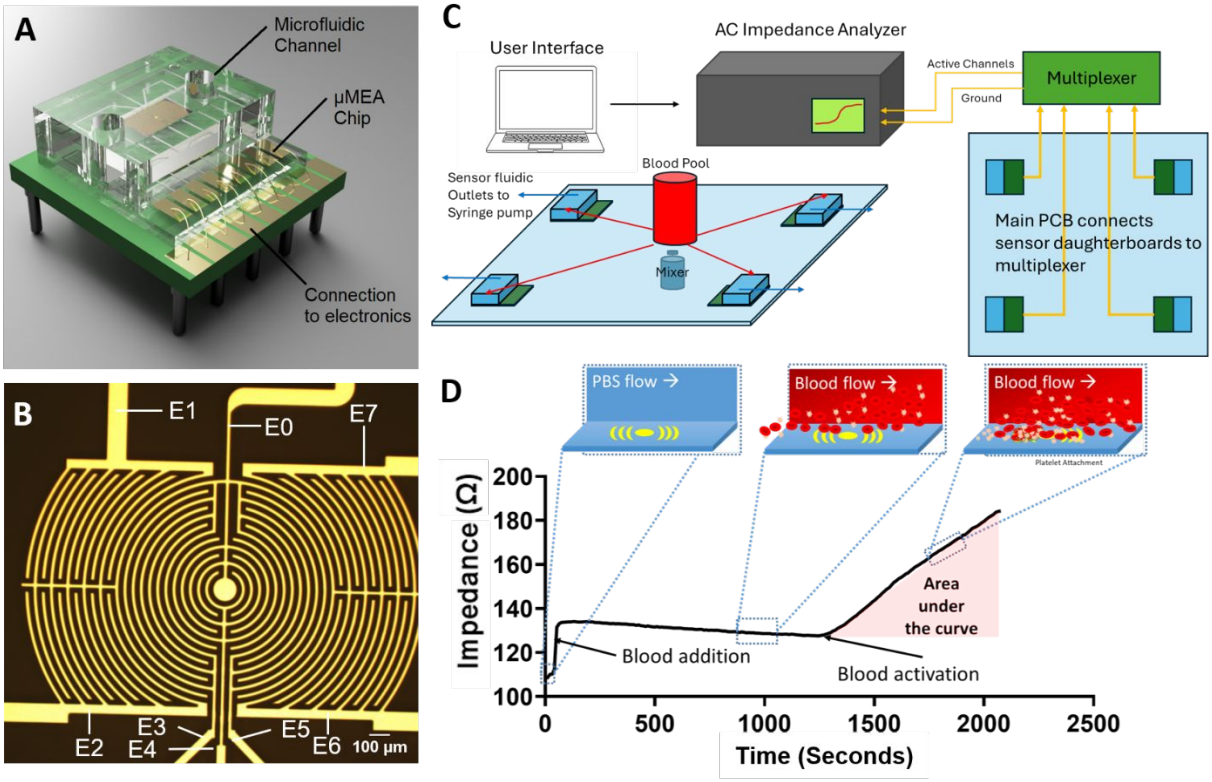

Figure 1. Illustration of sensor design, setup, and operation. (A) Rendered model of µMEA sensor unit comprising of glass µMEA chip, mounted PDMS microfluidic channel and electronics board. (B) µMEA interdigitated electrodes with labelled individual connections (E0-E7). (C) Schematic of benchtop setup indicating multiplexed measurement with four integrated µMEA chips. Blood flows from the common blood pool to the inlets of the chips (red arrows) and is perfused across the sensor surface via a syringe pump connected to the outlets (blue arrows).

The electrical readout from the pins of the μMEA chip (yellow arrows) are chosen via a multiplexer and read using a computer. (D) Trace of impedance magnitude generated at 150kHz from an ADP activated blood sample showing initial stabilization after blood addition and steady increase upon activation and platelet aggregation. Shown, in addition, are drawings indicating channel contents and the sensor surface at t = 0, 1000s and 1800s as well as AUC.

to four such packaged μMEA sensors can be integrated into a testing setup shown in Fig. 1(C) (and Fig. S1), where they are connected to a common sample source (i.e., a vial of stirred whole blood), the flow is control via tubing and a syringe pump, and the electronics for multiplexed, multi-frequency impedance measurement. The flow and impedance measurement are controlled by a custom-built MATLAB program running on a computer which displays real-time impedance data and stores it for downstream analysis.

On the μMEA chip, an electrode width and gap of 20μm was selected as a trade-off between providing sufficient resolution to pick up random or flow-driven systematic spatial variations in platelet aggregation across the channel surface while also providing inherent averaging over the granularity of individual cells and platelet aggregates and meeting needs of ease of fabrication. These dimensions also set the extent of penetration of the electric field in the channel at various measurement frequencies[28] whose height is set here using flow-related considerations discussed below. The design of the microelectrodes also enables high-resolution imaging of platelet aggregation on the chip surface from whole blood via electrode gaps through the thin and transparent glass substrate. Additionally, to quantify possible spatial heterogeneity and flow dependencies of platelet aggregation across channel, the electrode array was designed to allow focusing of impedance measurement to various sub-zones of the channel. As shown in Fig. 1(B), the electrode array consists of a single central (E0) and seven other separate (E1-E7) structures. These electrodes can be electronically selected in desired groupings, effectively allowing measurement of impedance change of different regions of the channel surface.

The microfluidic channel dimensions (rectangular cross-section with height h = 50μm and width w = 2.1mm) were designed to produce physiologically relevant blood shear rates ($\dot{\gamma}$~10-1000/s)[29]. Since shear rate increases rapidly with decreasing channel height, thin channels are preferred to obtain large shear rates

using reasonable flow rate. A lower limit on the channel dimensions is however set by the need to establish continuous clog-free flow during the measurement despite the formation of multicellular platelet microaggregates. While the size of the microaggregates can vary with shear rate, and chemical and biological assay parameters, a median size of ~20μm has been reported earlier[13]. Balancing these requirements, the channel height of 50μm was selected. Given that the flow rate Q used here is between 50μL/min and 100μL/min, the shear rate was calculated to be $\dot{\gamma}\sim\frac{6Q}{wh^2} =$ 952.4/s and 1904/s, where a parallel plate flow chamber approximation[30] was used. A computational model of the flow in the microchannel using COMSOL Multiphysics verifies a similar value for shear rates (Fig. S2) ($\dot{\gamma}\sim 831/s - 1660/s$).

Representative impedance measurement results of the μMEA sensor are shown in Fig. 1(D), where the impedance was measured at the frequency of 150kHz. Initially, the sensor was primed with 1X PBS buffer until a steady baseline impedance was reached. Then, the inlet was connected to the blood vial and blood entered the channel, the impedance value increased and then stabilized again. Adding the platelet activation reagent (ADP, 5μM) to the blood sample resulted in a continuous rise in impedance over time resulting from platelet aggregation. From this signal, metrics characterizing platelet aggregation such as Area under the Curve (AUC) were extracted.

Validation of Impedance Measurement with Simultaneous Fluorescence Imaging

We further performed fluorescence imaging simultaneously during impedance measurements to confirm that the observed impedance change, upon sample activation, was due to platelets aggregating on the chip surface. The experimental setup is shown in Fig. 2(A), where the μMEA sensor was mounted on a microscope stage and imaged from below, while electrical and flow connections were provided from above. Whole blood containing platelets labeled by 1mM mepacrine was used for these experiments. The fluorescence of the sensor surface was continuously monitored for the duration of the experiment.

During initial blood flow, rapid passage of labeled platelets was observed without any surface adhesion or resultant increase of surface fluorescence. Upon sample activation, platelets began adhering

and on the sensor surface, resulting in increased fluorescence intensity. Initial experiments showed that the number of platelet aggregates on the sensor surface, as measured by the fluorescence intensity, decreased along the direction of blood flow. To investigate whether this gradient correlates with impedance measurement, we measured and compared the impedance change of different zones of the electrode array. The impedances of two separate zones (i.e., one upstream (front) in the flow sensed by E1 and E2 electrodes connected together, and the other downstream (back) sensed by E6 and E7 electrodes connected together) and the overall electrode array as ground (E0), as shown in Fig. 2(B), were all monitored in a multiplexed manner, while the fluorescence signal of the whole area was monitored.

Fig. 2(C) shows the percentage change in impedance magnitude and fluorescence intensity, for each of the individual regions (front and back) as well as over the entire sensor (global). In general, the fluorescence and the impedance signals both show trends like the trace in Fig. 1(D), where a flat baseline is observed in the beginning and after the blood sample is activated, both signals simultaneously increase in all zones. Moreover, the correlation between the two signals was also examined. The Pearson's R

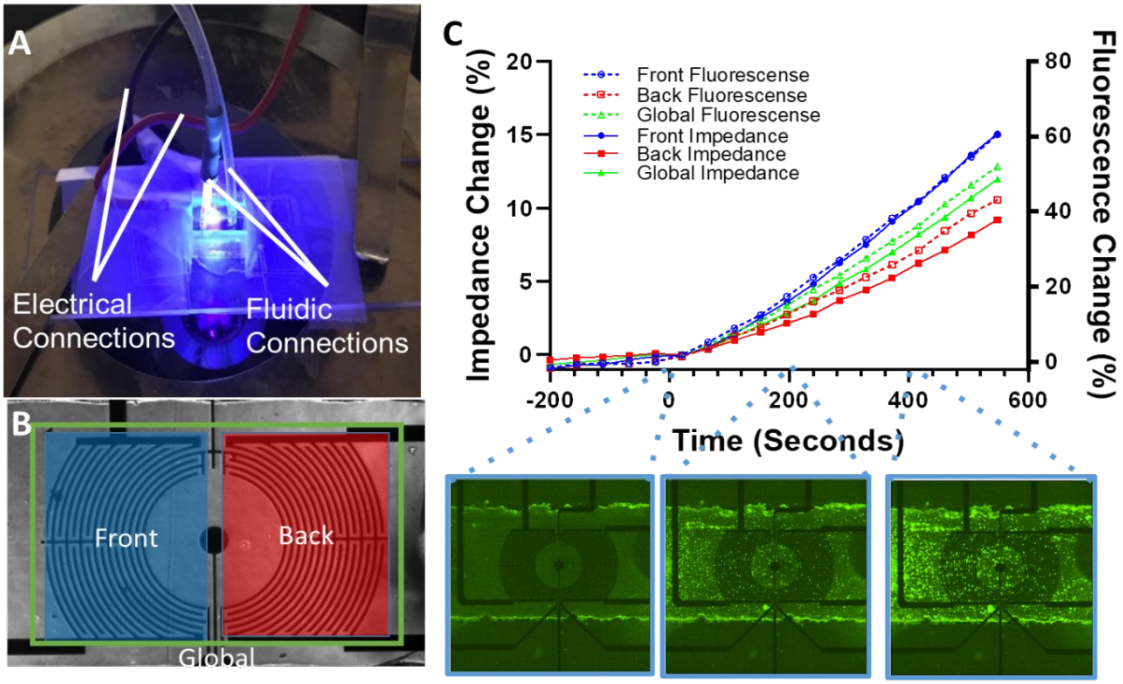

Figure 2. (A) Photograph of combined setup for fluorescence imaging and impedance measurement. Shown are, the μMEA sensor mounted on the microscope stage with top-down UV illumination as well as flow and electrical connections. (B) Micrograph of μMEA microelectrode array with measurement regions front, back and global labelled and shaded/outlined. (C) Plots of percentage change in impedance (continuous) and percentage change in fluorescence (dashed) vs. time from front, back and global regions. The insets are fluorescence micrographs showing platelet aggregation at t = 0, 200s and 400s. The time axis is adjusted such that t = 0 means when the sample was activated.

coefficient values for the two signals from the front, back and global measurements are 0.9992, 0.9985 and 0.9988 respectively ($p < 0.001$), indicating a strong correlation between the optical and electrical measurements of platelet aggregation. This further verifies that the label-free impedance aggregometry signal matches the direct optical measurement of platelet aggregates. To maximize electrical signal, front impedance (measured between E0 electrode as ground and E1 + E2 electrodes connected together) is used for following experiments.

Multi-Frequency μMEA Optimization

In contrast to conventional macroscale MEA, where the wire electrode impedance is measured at a single frequency[31], the μMEA platform is capable of measuring impedance across a broad range (e.g. from f = 1kHz to 2MHz) and from up to four sensors in parallel. Taking advantage of these features, we investigated the overall frequency response of the sensor, devised an equivalent-circuit model to explain it and then studied the influence of choice of frequency on sensor performance including sensitivity and repeatability.

Fig. 3(A) show the impedance magnitude and phase response of the μMEA sensor at different platelet aggregation states (e.g., pre-activation at t = 0, early-stage platelet aggregation at t = 345s, and late-stage platelet aggregation at t = 690s). The μMEA sensor exhibits a capacitive behavior in low frequency regime and then transitions to a resistive behavior at high frequencies. While the overall characteristics of the spectra remain consistent among the three time points, the results suggest that the effects of platelet aggregation could be more noticeable at certain intermediate frequencies. For example, when the frequency

is less than 50kHz, the impedance values measured at the three time points are almost the same, but they are more separated at frequency between 50kHz and 1000kHz.

These observations can be explained using an equivalent circuit model of the μMEA sensors in Fig. 3(B) which is adapted from an earlier reported model[32] of whole blood impedance spectroscopy. Based on the measured impedance spectra it can be inferred that in the low frequency range, C_{DL}, the double layer capacitance, dominates the overall sensor impedance. The contribution of the adhered platelets, likely dominated by the membrane capacitance, C_M, in this frequency range, is relatively low. At higher frequencies, the impedance of C_{DL} decreases, but the overall contribution of platelets to sensor impedance becomes significant. Finally at high frequencies, all capacitance elements are shorted, and the sensor is expected to behave as a pure resistor. Note that this may result in a relative reduction of the impedance contribution of the platelets as well at high enough frequencies.

We then used the capabilities of the μMEA sensor and system to understand the relationship between the change of impedance spectrum and platelet aggregation and investigate whether there is an optimal measurement frequency for high sensitivity and repeatability. Impedance spectra over time were captured from four chips each as technical replicates in two experimental runs (labeled as Run 1 and Run 2). Two separate activated blood samples (ADP, 5μM) were used in these serving as biological replicates.

Fig. 3(C) shows the AUC values (as defined above) calculated from the impedance transients up until time t = 500s at various frequencies. Curves for the intra-run averages for each experiment and the inter-run average are shown in the foreground, while curves for the individual technical replicates are in the background.

It was observed that the AUC first increases with frequency, reaching a maximum at ~400 kHz, and then decreases at higher frequencies. Also, a separate negative control experiment (labeled Cangrelor) was performed, with two chips as technical replicates, where the platelet inhibitor drug Cangrelor (100nM), a P2-Y12 receptor inhibitor[33], was added to the blood sample prior to the addition of ADP. Examining

impedance change for experiments with both active and inhibited blood over both time and frequency domains, Fig. 3(D) presents the comprehensive AUC information during platelet aggregation. While AUC is generally seen increasing with time across a broad frequency range (e.g., 10kHz to 1MHz), for the activated blood the rise of AUC measured at certain frequencies (e.g., 100kHz to 600kHz) could start earlier and be more significant, leading to better sensitivity for characterization of platelet aggregation. The drug-inhibited blood negative control experiment results in AUC curves that show little change across all time at all frequencies.

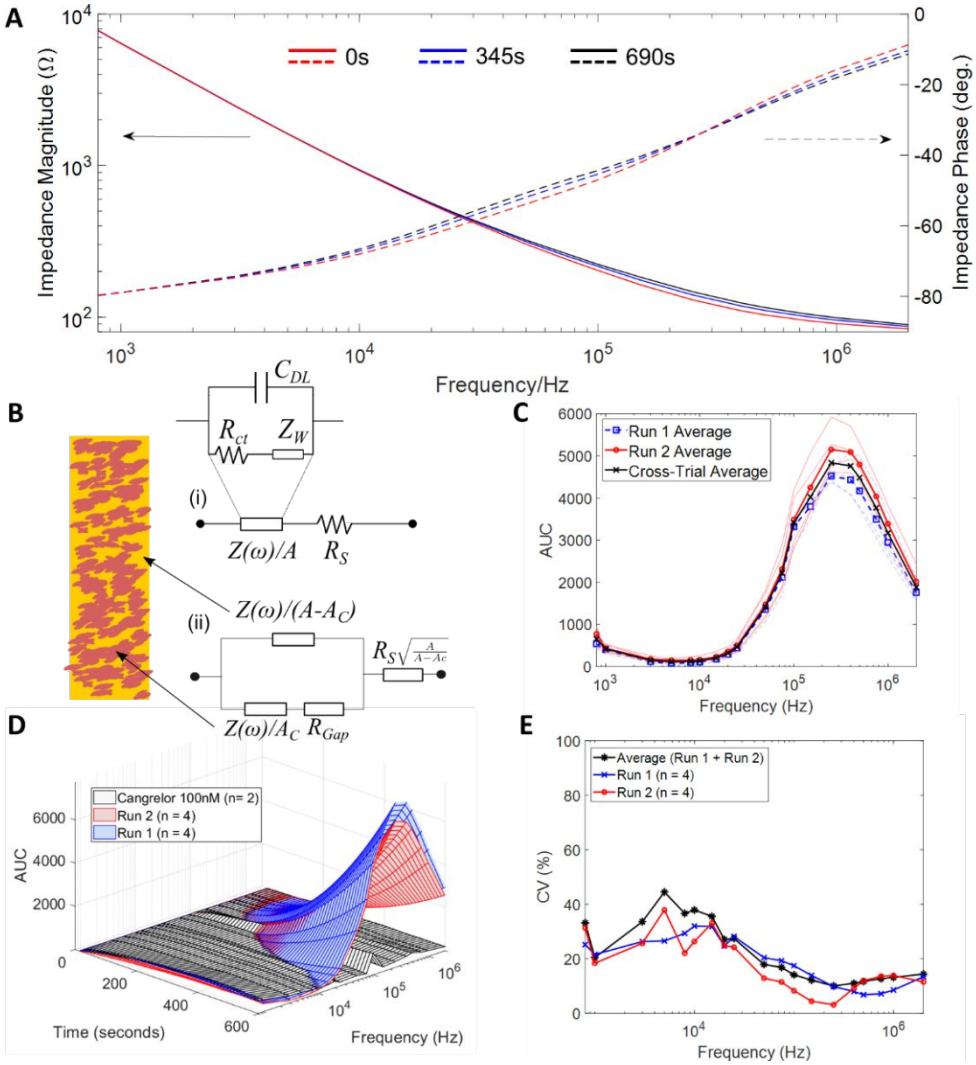

Figure 3. (A) Frequency response of μMEA sensor at three time points (t = 0, 345s and 690s) showing effect of platelet aggregation on electrical impedance magnitude (solid) and phase (dashed). (B) Equivalent circuit models for the bare electrode (i) and platelet adhered electrode (ii) surfaces of the μMEA sensor, where Z(ω): the electrode

surface impedance, A: total electrode surface area, A_c: electrode area covered by aggregates, C_{DL}: double layer capacitance, R_{ct}: the charge transfer resistance at the electrode-electrolyte interface, Z_w: the Warburg impedance modeling slow mass diffusion processes near the electrode surface, R_S: the spreading resistance, R_{Gap}: gap resistance from platelet-electrode interface. (C) Area under curve (AUC) vs. frequency at t = 500s, plotted for each run as well as the inter-run average. Graphs of individual trials are shown in the background for reference. (D) 3D Surface plot comparing the inter-run average AUC values of normal blood trials (Run 1 and Run 2) and those performed with Cangrelor in both time and frequency domain. (E) Coefficient of variation of AUC versus frequency.

In addition to AUC signal strength, we examined the influence of frequency on measurement precision, which was quantified here by the coefficient of variation (CV). Fig. 3(E) shows the CV of each experimental run and the overall inter-run average CV against frequency. The inter-run average CV is 20 – 45% at low frequency and drops to a minimal of 10% around 400kHz. Therefore, we selected 400kHz as the optimum frequency for impedance measurement.

Anti-Platelet Drug Response Measurement

Monitoring antiplatelet therapy is a key clinical application of platelet aggregometry[8,34]. As shown in Fig. 3(D), the μMEA sensor response under total inhibition via anti-platelet drugs, such as Cangrelor, is clearly distinguishable from the response obtained from normal blood samples. Therefore, to further characterize the performance of the μMEA sensor in monitoring anti-platelet therapy, drug dose response curves were constructed from blood samples, drawn from the same individual, activated using ADP (5μM) and incubated with varying Cangrelor concentrations. The percentage of aggregation (i.e., y axis in Fig. 4(A) and (B)) is defined as the ratio between the inhibited (at varying drug concentrations) and control (normal blood) responses.

In Fig. 4(A), the measurement frequency is fixed at 400kHz, typical downward sloping sigmoidal drug dose-response curves are observed, and the results also indicate that the time of measurement has minimal effect on the dose-response curves. In contrast, in Fig. 4(B), where AUC at a measurement time of 700s is used, the significant effect of measurement frequency is shown through the drastic change in the

curve slopes of the drug dose-response curves. The half maximal inhibitory concentration (i.e., IC50) and the dynamic range (i.e., the concentration range corresponding to the 5% to 95% interval of the response) were calculated from the dose response curves in Fig. 4(B) and are shown in Fig. 4(C) and (D), respectively. The measured IC50 of Cangrelor for platelet aggregation is found to be ~2nM, which is within the range of values reported in literature[35,36]. It is also observed that this value remains largely unchanged with measurement frequency for f < 1MHz. On the other hand, the dynamic range of the measurement increases throughout the entire range of measurement frequencies.

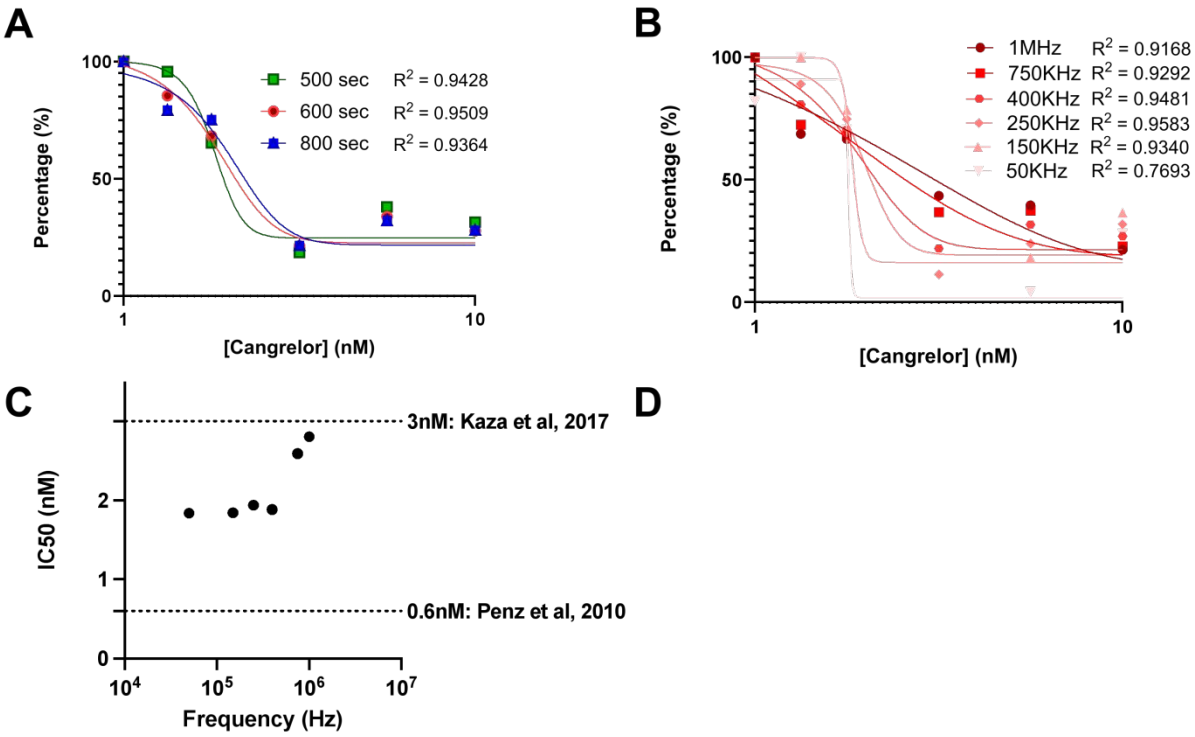

Figure 4. Anti-platelet drug response measurement. **(**A) Cangrelor dose response measured at *t*= 500s, 600s and 800s and *f* = 400kHz, where individual data points are shown with fitted dose response curves. (B) Cangrelor dose response studied at 50kHz, 150kHz, 250kHz, 400kHz, 750kHz and 1MHz and *t* = 700s, where individual data points are shown along with sigmoid best fit curves. (C) and (D) are the half maximal inhibitory concentration (IC50) and the dynamic range values of Cangrelor at multiple frequencies calculated from dose response curves in (B), respectively.

This tunable dynamic range of the sensor using measurement frequency is pertinent in clinical use for dose titration in patients using this sensor as a companion diagnostic, as the dynamic range of the sensor can be adjusted according to the concentration range of interest for the administered drug. Though the underlying reason for this frequency-dependent response requires further study, we hypothesize that this is related to the variation in the relative contribution of platelet aggregates bound on the electrode surface versus those free-floating in the flowing whole blood to the overall sensor impedance response with measurement frequency.

Thrombocytopenia Measurement

Thrombocytopenia, or a low number of platelets in blood, presents a challenge to assessing platelet function and is encountered frequently in the ICU[20]. Currently, commercial platelet aggregometers lack the sensitivity to measure thrombocytopenic samples and thus recommend against testing at platelet counts below 100,000/μL[7]. In contrast, by incorporating controlled blood flow and inter-digitated microelectrodes for sensitive and repeatable impedance measurements, our μMEA platform can potentially permit sensitive detection of platelet aggregates at such platelet counts. Therefore, we investigated the use of our platform for measurement of platelet aggregation from thrombocytopenic samples.

To this end, a low platelet model blood sample was prepared from normal whole blood following the platelet depletion procedures outlined in literature[26,27]. This low platelet model was then verified through complete blood count (CBC) measurement (Fig. 5(A)), which showed that it had platelet counts within the thrombocytopenic range. Furthermore, the red blood cells were preserved, as evidenced in Fig. 5(B) showing matching hematocrit levels in the model blood sample and normal blood samples. Fig. 5(C) compares the AUC signal measured using μMEA sensors from activated and inhibited whole blood samples (red, platelet count: 258 $\times 10^3/\mu L$) alongside the activated and inhibited low platelet count or thrombocytopenic blood model (blue, platelet count: $75 \times 10^3/\mu L$). The fluorescence images of the sensors confirm significantly lower number of platelet aggregates on the sensor surface used with the low platelet blood model. While conventional platforms have poor sensitivity at platelet concentrations as low as

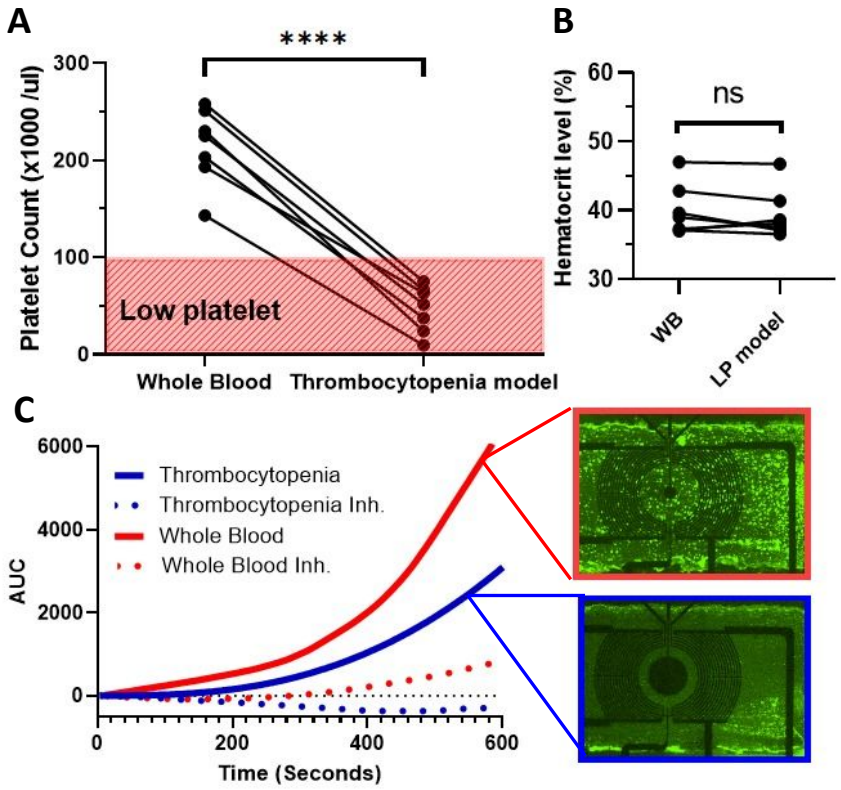

Figure 5. Thrombocytopenia measurement. (A) Validation of the thrombocytopenia model showing reduction of platelet count within thrombocytopenic range. (B) Preservation of red blood cells in thrombocytopenia/Low Platelet (LP) model shown by comparable hematocrit levels (difference is non-significant (ns)) to healthy blood samples. (C) Distinct differences in AUC magnitude between normal whole blood and thrombocytopenic model samples. Fluorescence micrographs are shown in insets to illustrate differences in aggregate formation across the chip surface.

100,000/μL[37], the μMEA platform's sensitivity, in the same platelet count range, is demonstrated by the thrombocytopenic blood signal being measurable and distinct from the drug-inhibited negative control response.

4. Discussion

The μMEA platform developed here addresses many of the limitations encountered by conventional macro-scale MEA platforms. The use of a two-dimensional microelectrode array embedded

in a microchannel improves the detection sensitivity of platelet aggregation through impedance measurement, permitting the μMEA sensor to measure platelet aggregation in samples in a label-free manner with less than 100,000/μL platelets and monitor platelet activity in thrombocytopenia. Additionally, one question commonly raised about conventional MEA is whether its measurements are representative of the in-vivo behavior of platelets because blood flow is missing during the measurement. We addressed this issue by performing aggregation measurement under constant flow at physiological shear rates. Testing under flow presents the additional benefit of continuously replenishing the blood volume near the sensor surface with new activated platelets, which not only better mimics the in-vivo blood clotting scenario, but also prevents platelet depletion which is commonly seen in testing with still samples.

Featuring electrode sub-arrays, the μMEA sensor can focus the impedance measurement to various subzones in the channel and thus provide more information to understand spatial variation in platelet activation. In our study, we found that the number of platelet aggregates on the sensor surface decreased along the direction of blood flow. Flow-driven gradient of surface-bound species has been observed in earlier work[10] and is attributed to reactant depletion in the context of molecular binding reactions with flow within microchannels. However, we note that a platelet depletion effect is unlikely in our case due to the high number of platelets in healthy blood (between 150,000/μL – 450,000/μL) relative to the number of bound aggregates observed. Instead, we hypothesize that gradient effect observed here could be a result of interaction of the blood flow and the changing morphology of the sensor surface as platelets aggregate. For example, upstream platelet buildup can alter the downstream flow of blood, pushing further arriving platelets away from the bottom surface of the channel reducing the aggregation in that downstream zone. While this mechanistic explanation has not been directly confirmed in the present study, we note that this has possible implications for the optimization of the sensor. This represents an opportunity for creating a further optimized flow environment to efficiently capture platelets across the entire surface of the sensor and thus further boost the sensitivity and repeatability.

As compared to single frequency measurement in macro-scale MEA, the μMEA platform can measure impedance across a broad frequency range. We used these properties to optimize the performance of the platform. We found the optimal frequency (400kHz) which gives the most sensitivity of detecting platelet aggregation is much larger than the operation frequency of the conventional MEA (15kHz). This could be due to smaller double layer capacitance on μMEA sensor. The measurement frequency was also found to affect the IC50 value and dynamic range of the antiplatelet drug dose-response curve. The impedance spectroscopy measurement can thus not only offer flexibility for optimization for various scenarios, including as a companion diagnostic for anti-platelet therapy, but also provide information for comprehensive understanding of platelet aggregation. For example, impedance spectroscopy has been employed to model and detect blood hematocrit and sedimentation[27]. We believe similar approach could be used in platelet function analysis.

It is worth noting that while our sensor is sensitive enough to detect platelet aggregation in thrombocytopenic samples, the AUC is reduced compared to samples with normal platelet counts. A systematic investigation of the effect of platelet count on the sensor readout is warranted in the future work.

5. Conclusion

In this work, we presented the design, development, and application of a microfluidic multiple aggregometry (μMEA) sensor that integrates microfluidic blood flow with sensitive label-free electrical impedance-based measurements of platelet aggregation using an interdigitated microelectrode array. The performance of the sensor was validated by experiments with whole human blood and by simultaneous optical and electrical measurements. Its application to clinically relevant use cases including platelet response measurement from low platelet count or thrombocytopenic blood and anti-platelet drug monitoring was also investigated. The μMEA sensor thus holds promise for sensitive POC platelet function analysis of whole blood samples. Future work needs to be focused on further detailed testing with larger numbers of blood samples from well-characterized clinical cohorts of patients to directly establish the utility

of μMEA in clinical decision making. Additionally, the system developed here needs further development from a lab-scale prototype to a testable point-of-care device in real-world clinical settings, such as automatic dilution.

Acknowledgements:

We acknowledge funding support from the National Science Foundation (NSF1722200) and National Institute of Health (1R43HL140686-01) under their respective SBIR grant programs. A.S. acknowledges support from the Bernie Marcus Foundation for the Bernie Marcus Early Career Professorship. X.Z. acknowledges support from the National Key R&D Program of China (No. 2022YFF1202000).

Conflict of Interest Statement:

X. Z., K. K., A. S. are co-founders of Atantares Corporation, F. L-J, V. R. G, J. S. and D.W. are employees of Atantares Corporation.

References:

1 K. Kolandaivelu, R. Swaminathan, W. J. Gibson, V. B. Kolachalama, K. L. Nguyen-Ehrenreich, V. L. Giddings, L. Coleman, G. K. Wong and E. R. Edelman, *Circulation*, 2011, **123**, 1400-1409.

2 K. King, L. P. Grazette, D. N. Paltoo, J. T. McDevitt, S. K. Sia, P. M. Barrett, F. S. Apple, P. A. Gurbel, R. Weissleder, H. Leeds, E. J. Iturriaga, A. Rao, B. Adhikari, P. Desvigne-Nickens, Z. S. Galis and P. Libby, *JACC Basic Transl. Sci.*, 2016, **1**, 73-86.

3 K. Rao and H. Holmsen, *Semin. Hematol.*, 1986, **23**, 102-118.

4 R. J. Flower, *Platelets*, 2018, **29**, 749-755.

5 C. J. Kim, J. Kim, J. S. del Río, D. Y. Ki, J. Kim and Y. K. Cho, *Lab Chip*, 2021, **21**, 4707-4715.

6 D. C. Cardinal and R. J. Flower, *J. Pharmacol. Methods*, 1980, **3**, 135-158.

7 A. Hanke, K. Roberg, E. Monaca, T. Sellmann, C. F. Weber, N. Rahe-Meyer and K. Görlinger, *Eur. J. Med. Res.*, 2010, **15**, 214-219.

8 R. Paniccia, E. Antonucci, N. Maggini, E. Romano, A. M. Gori, R. Marcucci, D. Prisco and R. Abbate, *Am. J. Clin. Pathol.*, 2009, **131**, 834-842.

9 D. Sibbing, S. Braun, S. Jawansky, W. Vogt, J. Mehilli, A. Schömig, A. Kastrati and N. von Beckerath, *Thromb. Haemost.*, 2008, **99**, 121-126.

10 Tóth, A. Calatzis, S. Penz, H. Losonczy and W. Siess, *Thromb. Haemost.*, 2006, **96**, 781-788.

11 Y. Roka-Moiia, S. Bozzi, C. Ferrari, G. Mantica, A. Dimasi, M. Rasponi, A. Santoleri, M. Scavone, F. Consolo, M. Cattaneo, M. J. Slepian and A. Redaelli, Int. J. Mol. Sci., 2020, **21**(4), 1174.

12 T. M. Squires, R. J. Messinger and S. R. Manalis, Nat. Biotechnol., 2008, 26, 417-426.

13 W. S. Nesbitt, E. Westein, F. J. Tovar-Lopez, E. Tolouei, A. Mitchell, J. Fu, J. Carberry, A. Fouras and S. P. Jackson, *Nat. Med.*, 2009, **15**, 665-673.

14 M. Li, N. A. Hotaling, D. N. Ku and C. R. Forest, *Plos. One*, 2014, **9**. e82493.

15 E. Westein, A. D. van der Meer, M. J. E. Kuijpers, J. P. Frimat, A. van den Berg and J. W. M. Heemskerk, *Proc. Natl. Acad. Sci.*, 2013, **110**, 1357-1362.

16 Jain, A. Graveline, A. Waterhouse, A. Vernet, R. Flaumenhaft and D. E. Ingber, *Nat. Commun.*, 2016, **7**, 10176.

17 M. Li, D. N. Ku and C. R. Forest, *Lab Chip*, 2012, **12**, 1355-1362.

18 S. Xu, J. Piao, B. Lee, C. Lim and S. Shin, *Biosensors & Bioelectronics*, 2020, **165**, 112395.

19 K. Harada, W. L. Wang and T. Shinozawa, *Sci. Rep.*, 2024, **14**, 14109.

20 T. S. Elgohary, H. E. Zaghla, A. Azab and T. Hagag, *Med. J. Cairo. Univ.*, 2011, **79**, 1-9.

21 G. J. Kuiper, R. Houben, R. J. Wetzels, P. W. Verhezen, R. v. Oerle, H. Ten Cate, Y. M. Henskens and M. D. Lancé, *Platelets*, 2017, **28**, 668-675.

22 D. C. Duffy, J. C. McDonald, O. J. Schueller and G. M. Whitesides, *Anal. Chem.*, 1998, **70**, 4974-4984.

23 B. Savage, F. Almus-Jacobs and Z. M. Ruggeri, *Cell*, 1998, **94**, 657-666.

24 M. K. Puurunen, S. J. Hwang, M. G. Larson, R. S. Vasan, C. J. O'Donnell, G. Tofler and A. D. Johnson, *J. Am. Heart. Assoc.*, 2018, **7**, e008522.

25 H. A. Hanby, J. L. Bao, J. Y. Noh, D. Jarocha, M. Poncz, M. J. Weiss and M. S. Marks, *Blood Adv.*, 2017, **1**, 1478-1490.

26 R. S. Bercovitz, M. K. Brenner and D. K. Newman, *Ann. Hematol.*, 2016, **95**, 1887-1894.

27 M. T. Skipper, P. Rubak, O. H. Larsen and A. M. Hvas, *Platelets*, 2016, **27**, 295-300.

28 N. S. Mazlan, M. M. Ramli, M. M. A. B. Abdullah, D. S. C. Halin, S. S. M. Isa, L. F. A. Talip, N. S. Danial and S. A. Z. Murad, *AIP Conf. Proc.*, 2017, 1885.

29 L. D. C. Casa, D. H. Deaton and D. N. Ku, *J. Vasc. Surg.*, 2015, **61**, 1068-1080.

30 C. Zhang and S. Neelamegham, *Platelets*, 2017, **28**, 434-440.

31 M. B. Zucker, *Methods Enzymol.*, 1989, **169**, 117-133.

32 A. Zhbanov and S. Yang, *Anal. Methods*, 2017, **9**, 3302-3313.

33 N. B. Norgard, *Expert Opin. Inv. Drugs*, 2009, **18**, 1219-1230.

34 R. Paniccia, E. Antonucci, N. Maggini, M. Miranda, A. M. Gori, R. Marcucci, B. Giusti, D. Balzi, D. Prisco and R. Abbate, *Thromb. Haemost.*, 2010, **104**, 287-292.

35 E. A. Kaza, M. C. Egalka, H. Zhou, J. Chen, D. Evans, J. Prats, R. Li, S. L. Diamond, J. A. Vincent, E. A. Bacha and T. G. Diacovo, *JACC Basic Transl. Sci.*, 2017, **2**, 465-476.

36 S. M. Penz, I. Bernlochner, O. Toth, R. Lorenz, A. Calatzis and W. Siess, *Thromb. J.*, 2010, **8**, 9.

37 E. I. Peerschke, D. D. Castellone, A. K. Stroobants and J. Francis, *Am. J. Clin. Pathol.*, 2014, **142**, 647-656.

The data supporting this article have been included as part of the Supplementary Information.